UNIVERSITY OF
BATH

**University of Bath**

# Ultraviolet four-wave mixing in the LP$_{02}$ fiber mode

**Y. Chen, W. J. Wadsworth, and T. A. Birks***

*Centre for Photonics and Photonic Materials, Department of Physics, University of Bath, BA2 7AY, UK*
*\*Corresponding author: t.a.birks@bath.ac.uk*

We report UV four-wave mixing in the LP$_{02}$ mode of a photonic crystal fiber when pumped by a frequency-doubled 532 nm microchip laser in the normal dispersion regime. A pure LP$_{02}$ mode was generated for the pump light by a broadband all-fiber mode converter. Ultraviolet signal wavelengths as short as 342 nm were generated.   © 2013 Optical Society of America

*OCIS codes:*   (060.4370) Nonlinear optics, fibers; (060.5295) Photonic crystal fibers; (060.2380) Fiber optics sources and detectors; (190.4380) Nonlinear optics, four-wave mixing.
http://dx.doi.org/10.1364/OL.38.003747

The generation of spatially coherent light in the UV and visible is important for applications including fluorescence spectroscopy and fluorescence imaging. Relatively few wavelengths in this region are readily available from laser sources, and many avenues have been explored for wavelength conversion of existing lasers into this region. Nonlinearity in optical fibers can fulfil some of the requirements of tunable or selectable wavelengths, and four-wave mixing (FWM) from 1550, 1064, and 800 nm sources is well established. Its applications include pulse generation, broadband optical amplification [1], and optical parametric oscillators [2].

The control over nonlinearity and dispersion that is provided by photonic crystal fibers (PCFs) [3–5] has enabled FWM in PCF to be used for high-power red and near-infrared sources [6–10]. However, generation of discrete new wavelengths in the UV range remains difficult. FWM clearly cannot directly generate wavelengths shorter than half the pump wavelength, and it is usually limited to much longer wavelengths. For example, the shortest wavelengths available from 1064 nm pumping are beyond 600 nm [9,10]. Although this output may then be frequency doubled to the UV [11], this adds complexity to the system.

UV generation directly by FWM requires a pump in the green or blue. Furthermore, for FWM in fiber to generate signal and idler wavelengths widely separated from the pump, the pump wavelength must be close to but shorter than the zero dispersion wavelength (ZDW) of the fiber [3,4,9–11]. In PCF the ZDW is shortest when the holes are large, and is then determined mainly by the core diameter [5]. A core diameter of around 0.9 μm is needed for a ZDW of 532 nm in the fundamental mode [12,13]. However, PCFs with such small cores are difficult to draw and are susceptible to high loss, two-photon absorption, and damage at high powers [14]. This limits the shortest wavelength obtainable by FWM.

Alternative phase-matching schemes can overcome the difficulty of designing fibers for pumping at 532 nm, including dual-wavelength pumping at 532 and 1064 nm [15,16] and birefringent or intermodal phase matching [15,17,18], but none has been able to generate light below 400 nm. Non-FWM UV output has been observed using femtosecond lasers at 800 nm but in uncontrolled high-order modes with no scheme for fundamental-mode output [19]. One may argue that pumping FWM at 532 nm (from a frequency-doubled laser) requires the same

sequential nonlinearities of second-harmonic generation (SHG) and FWM as frequency doubling of a 1064-nm-pumped FWM process, but intracavity SHG is so efficient and well engineered that 532 nm can in practice be regarded as a primary laser. Dispersive wave generation from ultrashort pulses in gas-filled fibers [20] can yield wavelengths below 300 nm, but requires a complex microjoule, sub-100-fs laser source.

Here, we report FWM in PCFs but entirely within the LP$_{02}$ higher-order mode. The enhanced waveguide dispersion of higher-order modes gives short ZDWs even with relatively large cores. For example, a core diameter as large as 2.7 μm gives a ZDW of 532 nm for the LP$_{02}$ mode [12]. FWM in higher-order modes not only permits the use of 532 nm pump light in robust structures, but the shape of the dispersion curves makes it easier to target a particular pump and signal wavelength. To predict the signal and idler wavelengths as functions of the pump wavelength and ZDW, phase-matching curves were calculated, Fig. 1, from momentum and energy conservation [3,6]:

$$2\beta_p = \beta_s + \beta_i + 2\gamma P \tag{1}$$

and

$$2\omega_p = \omega_s + \omega_i, \tag{2}$$

where $\beta_j$ and $\omega_j$ are the propagation constants and angular frequencies of the pump, signal, and idler in the appropriate mode, $\gamma = n_2 \omega_0 / c A_{\text{eff}}$ is the nonlinear coefficient, $A_{\text{eff}}$ is the effective area of the mode and $n_2 = 2 \times 10^{-20}$ m$^2$/W is the nonlinear refractive index [3]. Here, the PCFs are approximated by strands of silica surrounded by air [13], representing the most favorable limit of large air holes.

For visible wavelength pumping, Fig. 1 shows that the FWM wavelengths are much more sensitive to both pump wavelength and core diameter for LP$_{01}$ than for LP$_{02}$. FWM in the LP$_{01}$ mode in this regime has therefore not been demonstrated, because it is very difficult experimentally to achieve a combination of pump wavelength and fiber which gives rise to FWM rather than supercontinuum [13]. As well as being less sensitive to pump wavelength and diameter, FWM in the LP$_{02}$ mode also offers the opportunity to use shorter pump wavelengths (down to ~350 nm, compared with 470 nm for LP$_{01}$), and for a given pump wavelength offers shorter signal wavelengths
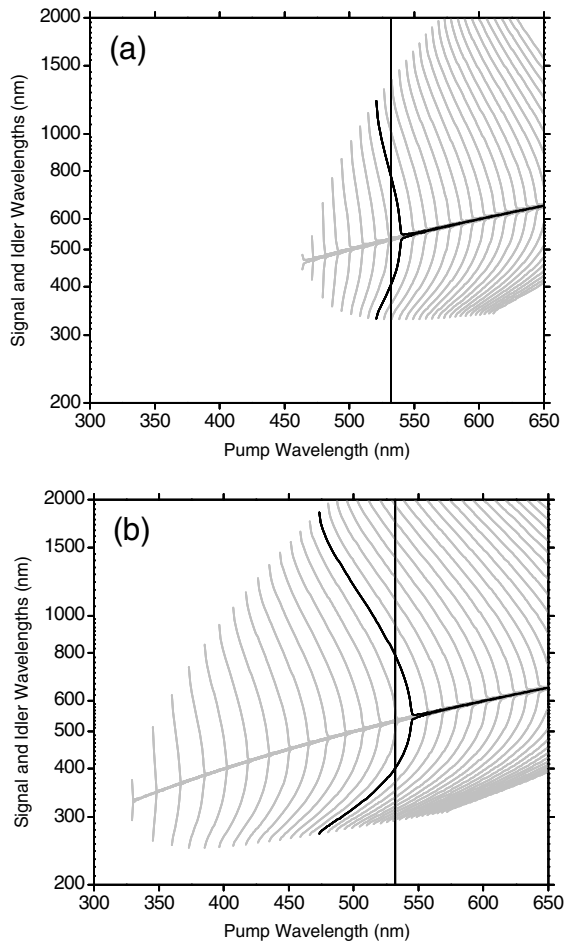
Fig. 1. Calculated phase-matching curves for (a) the $HE_{11}$ ($LP_{01}$) mode and (b) the $HE_{12}$ ($LP_{02}$) mode of a strand of silica in air, giving the signal and idler wavelengths as functions of pump wavelength for particular diameters. The thicker curves are for diameters of (a) 0.952 μm and (b) 2.86 μm, in each case chosen to generate 400 and 800 nm light for a 532 nm pump. The thinner curves are for increments of 5% diameter of the thick curves, increasing from left to right [0.571 to 1.90 μm in (a) and 0.858 to 5.72 μm in (b)]. $\gamma P$ is set to an arbitrarily low value.
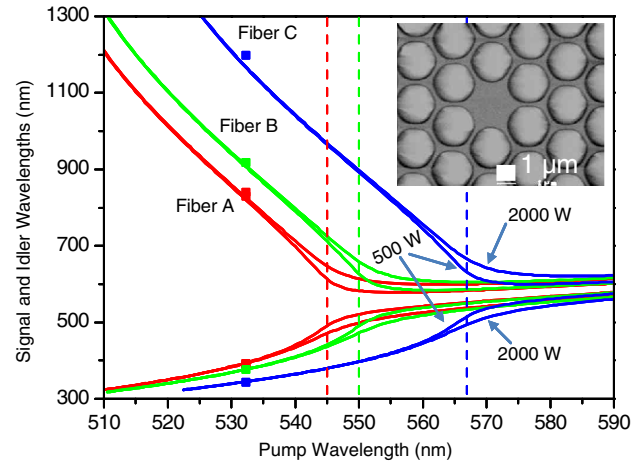


Fig. 2. Nonlinear phase matching for fibers A, B, and C. Solid lines are calculations for peak pump powers of 500 and 2000 W. Points are experimental results for a 532 nm pump laser. Dashed lines are the ZDWs. Inset is an SEM image of fiber B.

The phase-matching curves are of similar shape for fibers A, B, and C but with ZDWs at 545, 550, and 567 nm, respectively. Pump light with a wavelength shorter than ZDW, where dispersion is normal, will be converted to widely separated signal and idler wavelengths in the UV and near-IR, respectively. In this wavelength range, changing peak pump power in Eq. (1) from 500 to 2000 W has little effect on the predicted signal and idler wavelengths.

These calculations were tested using a frequency-doubled Nd:YAG microchip laser as the pump source (*Teem Photonics* NG-10320, 0.6 ns pulse duration at 532 nm, 7 kHz repetition rate, 24 mW average power). The pump pulses were coupled into each fiber via neutral-density filters, a polarizer, and a half-wave plate to control input power and polarization, Fig. 3. At the start of each fiber was a mode filter to ensure a pure fundamental $LP_{01}$ mode, followed by a low-loss all-fiber broadband $LP_{02}$ mode converter formed *in situ* within the fiber. For details of structures and coupling efficiencies see [12], which reports supercontinuum generation in the same mode. To avoid any nonlinear effects in the $LP_{01}$ mode before conversion to the $LP_{02}$ mode, the distance of $LP_{01}$ mode propagation was kept shorter than 20 cm. Mode patterns at the pump and FWM wavelengths were examined at the output end of the fiber using a grating and/or bandpass filters. Output spectra were recorded with an optical spectrum analyzer (OSA, *Ando* AQ6315B), but for wavelengths shorter than the 350 nm

(below 300 nm when pumped at 532 nm, compared with ~350 nm for $LP_{01}$).

To demonstrate FWM in the $LP_{02}$ mode experimentally, three few-mode PCFs with similar structures but slightly different core sizes were drawn from a common preform. When each fiber was pumped with 532 nm light in the $LP_{02}$ mode, FWM peaks were seen at UV (signal) and near-IR (idler) wavelengths, all outputs also being in the $LP_{02}$ mode.

Phase-matching curves for the $LP_{02}$ mode in the three PCFs, Fig. 2, were calculated as in Fig. 1 but for an actual PCF structure rather than a strand-of-silica approximation. $LP_{02}$ mode $\beta$ values were calculated by a plane wave method [6,21] based on dimensions measured from the scanning electron microscope (SEM) images of the PCFs. The hole diameter $d$, pitch $\Lambda$, and inscribed-circle core diameter were, respectively, 2.03, 2.28, and 2.43 μm for fiber A, 2.15, 2.39, and 2.49 μm for fiber B, and 2.19, 2.46, and 2.68 μm for fiber C. (The core diameters were smaller than $2\Lambda - d$ because the innermost six holes were slightly elongated toward the core.)
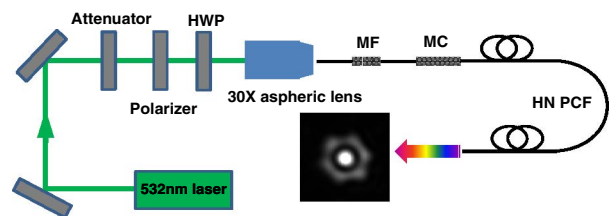


Fig. 3. Experimental setup. HWP, half-wave plate; MF, mode filter; MC, mode converter. Inset: typical near-field mode pattern at 532 nm.

limit of the OSA a UV spectrometer (*Ocean Optics* USB4000) was used instead.

Figure 4 shows output spectra for 2 m of $LP_{02}$-mode propagation in fiber A. The ~140 ps calculated walk-off between pump and idler pulses for this length of fiber is much less than the pump pulse duration (pump-signal and signal-idler walk-off are smaller). The calculated signal and idler wavelengths were 393 and 824 nm, respectively, and the observed signal wavelength was 390 nm. This demonstrates that the plane wave calculation based on the SEM image was sufficiently accurate to predict FWM wavelengths, which is fortunate because the dispersion of higher-order modes is difficult to measure directly [22].

For low pump power we see FWM peaks rise just above the background noise at locations well-separated from the pump wavelength. Around the pump wavelength there are also two stimulated Raman scattering (SRS) Stokes peaks at 545 and 558 nm and an anti-Stokes peak at 520 nm at about 15 dB less intensity than the 545 nm Stokes. Amplification of the anti-Stokes peak is due to weak coupling between SRS and FWM, as has been observed in the fundamental mode [7].

At an output power of 1.6 mW (~400 W coupled peak power) the signal remains narrowband (FWHM = ~1 nm), Figs. 4 and 5(a). The Raman Stokes wavelengths near the pump wavelength are longer than the ZDW in this fiber, and have sufficient power to form a continuum [6,23]. Cascaded Raman peaks appeared in the signal after just a slight increase of output power to 1.7 mW, indicating sufficient UV power to generate new wavelengths. This can be alleviated by shortening the fiber to an appropriate length for the particular pump power [9]. The idler is in the anomalous dispersion regime of the fiber, and we attribute its long-wavelength broadening to pulse breakup and the formation of Raman-shifting solitons. As well as the expected FWM, Fig. 4 shows weak sidebands at other wavelengths, such as those at 482 and 595 nm in Fig. 4.

**Table 1. Theoretical (Th.) and Experimental (Exp.) Fiber Parameters and FWM Peaks**

| Fiber | ZDW (nm) Th. | Signal (nm) Th. | Signal (nm) Exp. | Idler (nm) Th. | Idler (nm) Exp. |
|---|---|---|---|---|---|
| A (test 1) | 545 | 393 | 390 | 824 | 839 |
| A (test 2) | 545 | 393 | 392 | 824 | 829 |
| B | 550 | 376 | 375 | 910 | 918 |
| C | 567 | 344 | 342 | 1171 | 1198 |

These are not measurement artifacts and are consistent with an energy-conserving FWM process pumped at 532 nm, but we do not yet understand the corresponding phase-matching condition.

The near-field mode patterns at the pump and FWM wavelengths were checked regularly during the experiments and showed $LP_{02}$ mode purity of ~20 dB throughout, as determined by measurement of the intensity node [24]. Discrete images were made at wavelengths for which we have 10 nm bandpass filters, Fig. 4, and dispersed images produced by a diffraction grating provided information across all wavelengths.

To test for fiber uniformity, another mode filter and mode converter were made in a new section of fiber A and the experiment was repeated. Small differences in the FWM wavelengths were observed, Table 1. These correspond to a variation in fiber dimensions of around 0.2%, which is consistent with the uniformity of the fiber drawing process and potentially provides a way to measure core diameter variations to an accuracy of a few nanometers.

We repeated the experiment using fiber B, which had a slightly longer ZDW. The device had 1.7 m of $LP_{02}$ propagation after the mode converter. The signal and idler were more widely separated than in fiber A, as expected from the phase-matching curve in Fig. 2. The signal spectrum, with a peak at 375 nm, is shown in Fig. 5(b). For
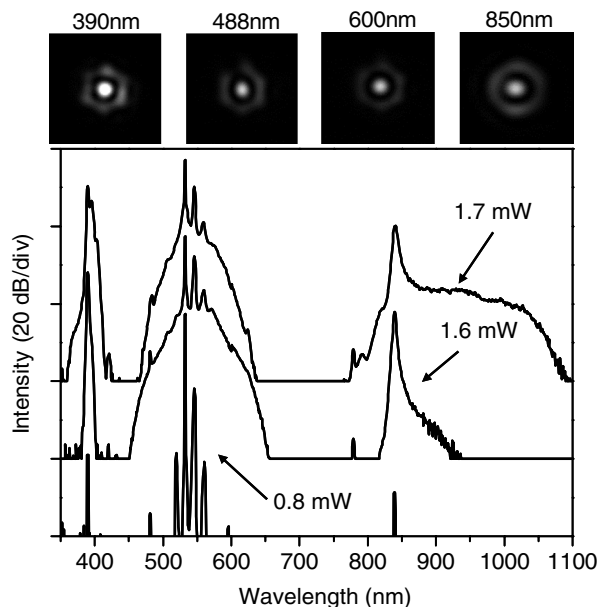


Fig. 4. Output spectra at different output powers in 2 m of fiber A. Resolution is 2 nm, each spectrum is vertically offset by 20 dB for clarity. Top row: output near-field patterns at selected wavelengths.
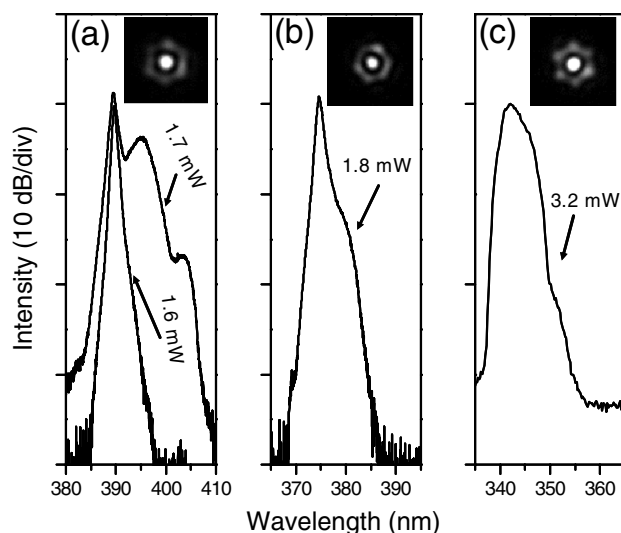


Fig. 5. (a), (b), (c) Signal spectra for fibers A, B, and C, respectively, at specific output powers. (a) and (b) were recorded by an OSA, (resolution 0.2 nm) while (c) was obtained by a UV spectrometer (resolution 1.3 nm). Insets: output near-field images at the signal wavelengths.

1.7 m of $LP_{02}$ mode propagation in fiber C, which had an even longer ZDW, the signal wavelength was shorter still at 342 nm, Fig. 5(c). In this case the calculated walk-off between pump and idler pulses was 330 ps, more than twice that of fiber A, and the calculated FWM gain bandwidth was also narrower. The wavelength conversion efficiency was therefore reduced and we did not observe any Raman Stokes line in the signal, even for a total output power of 3.2 mW.

UV power measurements were challenging for the low powers in our experiments. We measured the total output power for fiber B with and without a UV bandpass filter. The measured powers were 90 μW and 1.6 mW, respectively, corresponding to a conversion efficiency of about 6%. Unfortunately the long wavelength transmission edge of the filter coincided with the peak signal wavelength of 375 nm so this measurement is an underestimate—the real value should be rather higher. However, the easily observed cascaded Raman peaks in the signal peaks of fibers A and B indicate high conversion efficiency to short wavelengths.

In conclusion, we have experimentally demonstrated parametric FWM in the $LP_{02}$ mode via low-loss mode convertors pumped by a pulsed 532 nm laser. This provides an efficient way to generate well-defined UV wavelengths using an inexpensive source. If necessary, all three light waves could be converted back to the fundamental mode by a reversed mode converter at the output [12]. Applications for light of such wavelengths include fluorescence microscopy.

## References

1. J. Hansryd, P. A. Andrekson, M. Westlund, J. Li, and P. Hedekvist, IEEE J. Sel. Top. Quantum Electron. **8**, 506 (2002).
2. S. Coen and M. Haelterman, Opt. Lett. **26**, 39 (2001).
3. G. P. Agrawal, *Nonlinear Fiber Optics*, 4th ed. (Academic, 2007).
4. J. D. Harvey, R. Leonhardt, S. Coen, R. Leonhardt, G. K. L. Wong, J. C. Knight, W. J. Wadsworth, and Ph. St. J. Russell, Opt. Lett. **28**, 2225 (2003).
5. J. C. Knight, J. Arriaga, T. A. Birks, A. Ortigosa-Blanch, W. J. Wadsworth, and P. St. J. Russell, IEEE Photon. Technol. Lett. **12**, 807 (2000).
6. W. J. Wadsworth, N. Joly, J. C. Knight, T. A. Birks, F. Biancalana, and P. St. J. Russell, Opt. Express **12**, 299 (2004).
7. S. Coen, A. H. L. Chau, R. Leonhardt, J. D. Harvey, J. C. Knight, W. J. Wadsworth, and P. St. J. Russell, J. Opt. Soc. Am. B **19**, 753 (2002).
8. C. Xiong, Z. Chen, and W. J. Wadsworth, J. Lightwave Technol. **27**, 1638 (2009).
9. L. Lavoute, J. C. Knight, P. Dupriez, and W. J. Wadsworth, Opt. Express **18**, 16193 (2010).
10. D. Nodop, C. Jauregui, D. Schimpf, J. Limpert, and A. Tünnermann, Opt. Lett. **34**, 3499 (2009).
11. P. J. Mosley, S. A. Bateman, L. Lavoute, and W. J. Wadsworth, Opt. Express **19**, 25337 (2011).
12. Y. Chen, Z. Chen, W. J. Wadsworth, and T. A. Birks, Opt. Express **21**, 17786 (2013).
13. S. G. Leon-Saval, T. A. Birks, W. J. Wadsworth, P. St. J. Russell, and M. W. Mason, Opt. Express **12**, 2864 (2004).
14. M. Delgado-Pinar, P. J. Mosley, J. C. Knight, T. A. Birks, and W. J. Wadsworth, *Nonlinear Photonics Topical Meeting* Karlsruhe (2010), paper NWD3.
15. E. Räikkönen, S. C. Buchter, and M. Kaivola, Appl. Phys. B **91**, 461 (2008).
16. V. Tombelaine, P. Leproux, V. Couderc, and A. Barthélémy, IEEE Photon. Technol. Lett. **18**, 2466 (2006).
17. S. Wabnitz, A. Tonello, S. Pitois, G. Millot, T. Martynkien, W. Urbańczyk, J. Wójcik, A. Locatelli, M. Conforti, and C. De Angelis, Proc. SPIE **6612**, 66120D (2006).
18. P. Dupriez, F. Poletti, P. Horak, M. N. Petrovich, Y. Jeong, J. Nilsson, D. J. Richardson, and D. N. Payne, Opt. Express **15**, 3729 (2007).
19. A. Efimov, A. J. Taylor, F. G. Omenetto, J. C. Knight, W. J. Wadsworth, and P. St. J. Russell, Opt. Express **11**, 910 (2003).
20. J. C. Travers, W. K. Chang, J. Nold, N. Y. Joly, and P. St. J. Russell, J. Opt. Soc. Am. B **28**, A11 (2011).
21. G. J. Pearce, T. D. Hedley, and D. M. Bird, Phys. Rev. B **71**, 195108 (2005).
22. P. Nandi, Z. Chen, A. Witkowska, W. J. Wadsworth, T. A. Birks, and J. C. Knight, Opt. Lett. **34**, 1123 (2009).
23. J. M. Dudley, L. Provino, N. Grossard, H. Maillotte, R. S. Windeler, B. J. Eggleton, and S. Coen, J. Opt. Soc. Am. B **19**, 765 (2002).
24. K. Lai, S. G. Leon-Saval, A. Witkowska, W. J. Wadsworth, and T. A. Birks, Opt. Lett. **32**, 328 (2007).